LBL-19641 c.2

Lawrence Berkeley Laboratory

UNIVERSITY OF CALIFORNIA

RECEIVED
LAWRENCE
BERKELEY LABORATORY
JAN 14 1986
LIBRARY AND
DOCUMENTS SECTION

Engineering Division

Presented at the 1985 IEEE Nuclear Science Symposium, San Francisco, CA, October 21-25, 1985; and to be published in the Proceedings

300-ELEMENT SILICON-LITHIUM POSITION-SENSITIVE IMAGING DETECTOR FOR ANGIOGRAPHY

J.T. Walton, H.A. Sommer, A.C. Thompson,
E.B. Hughes, and H.D. Zeman

October 1985

TWO-WEEK LOAN COPY
This is a Library Circulating Copy
which may be borrowed for two weeks.

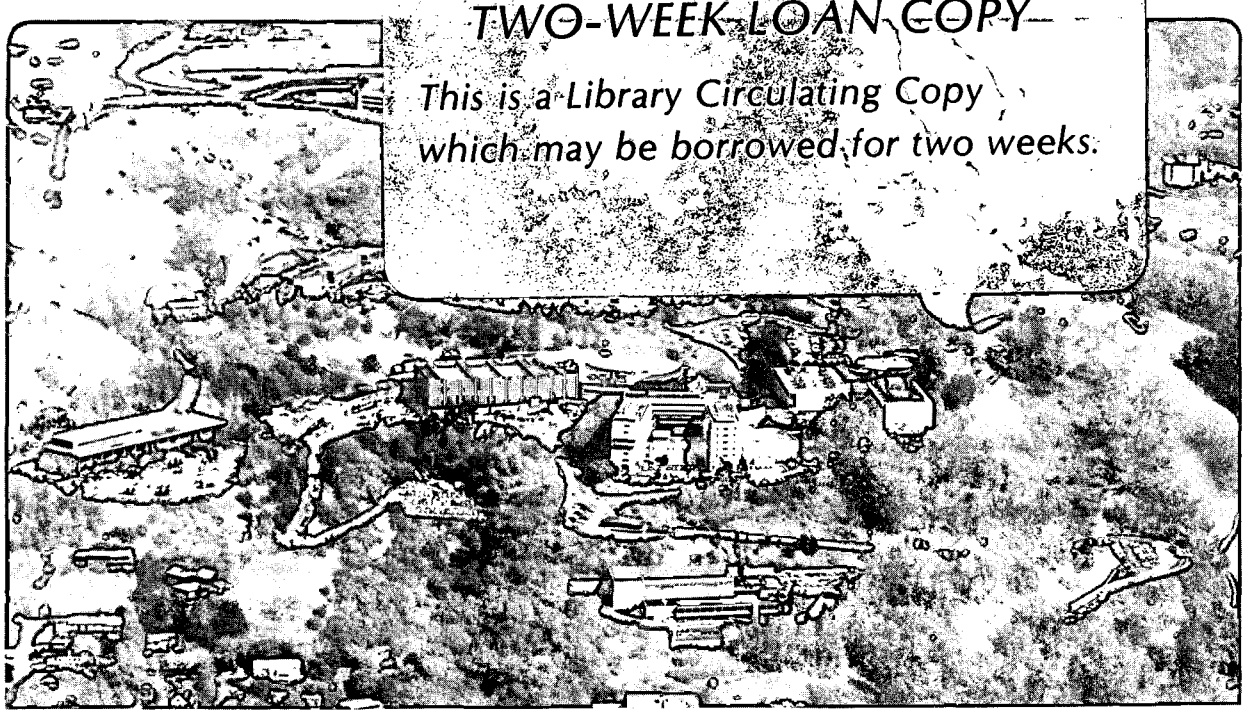

Prepared for the U.S. Department of Energy under Contract DE-AC03-76SF00098

LBL-19641 c.2

DISCLAIMER

This document was prepared as an account of work sponsored by the United States Government. While this document is believed to contain correct information, neither the United States Government nor any agency thereof, nor the Regents of the University of California, nor any of their employees, makes any warranty, express or implied, or assumes any legal responsibility for the accuracy, completeness, or usefulness of any information, apparatus, product, or process disclosed, or represents that its use would not infringe privately owned rights. Reference herein to any specific commercial product, process, or service by its trade name, trademark, manufacturer, or otherwise, does not necessarily constitute or imply its endorsement, recommendation, or favoring by the United States Government or any agency thereof, or the Regents of the University of California. The views and opinions of authors expressed herein do not necessarily state or reflect those of the United States Government or any agency thereof or the Regents of the University of California.

300-ELEMENT SILICON-LITHIUM POSITION-SENSITIVE IMAGING DETECTOR FOR ANGIOGRAPHY

J. T. Walton[1], H. A. Sommer[1], A. C. Thompson[1], E. B. Hughes[2] and H. D. Zeman[2]
[1]Lawrence Berkeley Laboratory
University of California
Berkeley, CA 94720 U.S.A.
and
[2]Hansen Laboratory of Physics
Stanford University
Stanford, CA 94305 U.S.A.

Abstract

Silicon lithium-drifted [Si(Li)] detectors 150 mm long, 10 mm wide and 5 mm thick with 300 individual elements have been fabricated as imaging detectors for noninvasive studies of human coronary arteries using 33 keV x-rays from a synchrotron radiation beamline. This detector is an extension of earlier work on 30 mm long devices with initially 30 and later 60 elements.

The detector fabrication details are discussed highlighting problems in uniform lithium-ion compensation. The device structure is examined and measurements on the interelement impedances presented. Finally an angiograph of the coronary arteries in an excised pig's heart obtained with this 300-element detector is presented.

Introduction

We have earlier reported on the use of silicon lithium-drifted [Si(Li)] detectors for application in medical imaging and, in particular, noninvasive imaging atherosclerotic lesions in human coronary arteries[1,2]. While these earlier papers focused on the application of Si(Li) detectors in noninvasive angiography, here we will mainly discuss the design and fabrication of these devices. The detectors reported on are Si(Li) devices 150 mm long, 10 mm wide and 5 mm thick with 300 individual elements. Our earlier work was with detectors 30 mm long, 10 mm wide and 5 mm thick with initially 30 and later 60 elements. The newer, longer devices are required to produce angiographs of the human heart.

While the size alone of these 300-element Si(Li) detectors makes them unique, the use of a guard-ring structure on the blocking contact is also a departure from normal practice[3]. The fabrication of these devices presented problems in material selection, processing, and evaluation. These will be discussed in the following.

Fabrication

Material Selection

At the present time, floating-zone, 1000 - 2000 ohm-cm p-type silicon crystals suitable for Si(Li) detector fabrication are limited, for the most part, to less than 80 mm in diameter. Consequently, the fabrication of the 300-element, 150 mm long detectors required that we cut the blanks from along the crystal axis. Since the normal crystal orientation employed with Si(Li) detectors is [111], the blanks were cut along the [111] crystal axis.

Prior to cutting the 150 mm long blanks from the silicon crystal, we evaluated the suitability of the crystal by slicing several wafers (i.e. cutting perpendicular to the [111] axis) and fabricating conventional 5 mm thick, 100 mm^2 detectors[4]. These test devices were successfully lithium-ion compensated. Further, in very limited studies, no crystal orientation dependency on the lithium-ion mobility has been observed. Consequently, when we then proceeded to fabricate the

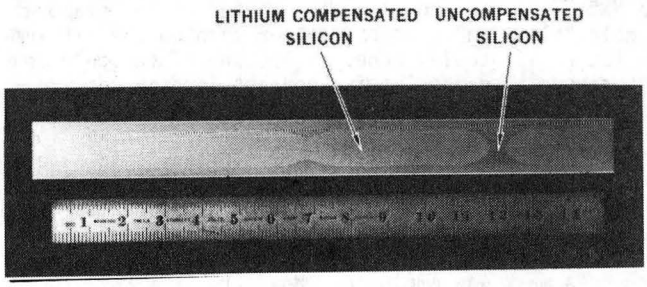

XBB 854-3108A

Fig. 1. Lithium-ion-compensated regions revealed by copper staining on a 150 mm long detector. The uncompensated region at about 12 cm on the accompanying scale indicates that there are defects present in the crystal which are degrading the lithium ion mobility.

150 mm long devices, the lithium-ion compensation results, as revealed by copper staining[5] and shown in Fig. 1, were unexpected. This figure shows that the lithium-ion compensation is dependent, in this crystal, on the axial location. While we have long suspected that certain individual wafers cut from a crystal may possess defects affecting the lithium-ion mobility, Fig. 1 clearly shows that there are regions along this crystal where the lithium-ion mobility is severely reduced. In dealing with individual wafers it can always be argued that detector processing variations deleteriously affected the lithium-ion mobility. However, here each of the four companion 150 mm long detectors fabricated on blanks cut from this crystal section exhibited a very similar pattern to that of Fig. 1, thereby conclusively demonstrating that the lithium-ion mobility is affected by defects present in the crystal.

We have earlier reported[6] and discussed some effects of crystal growth rate on the formation of A- and B-type swirl defects in floating-zone silicon. In our discussion of these defects we concluded that the formation of B-type swirls in sufficient density could reduce the lithium-ion mobility in a silicon crystal.

The stain pattern shown in Fig. 1 strongly resembles the shape of the molten zone present in the floating-zone process and therefore suggests that the defects which are reducing the lithium-ion mobility in these regions were introduced into the crystal by some mechanical perturbation of the crystal growth conditions. By measuring the depth of the lithium compensated region we have estimated that the lithium-ion mobility in these perturbed regions is reduced by a maximum of about 50% from the expected value. Similar reduced values for the lithium-ion mobility have been reported by Guislain, et al[7]. We have interpreted their results as indicating the presence of B-type swirl defects.

Since the stain pattern in Fig. 1 suggests mechanically induced defects, and the measured lithium-ion mobility is similar to published mobilities in silicon with B swirls, we conclude that B-swirl defects are

present in regions of this crystal in sufficient density to impede the lithium-ion mobility. While other sections of this crystal exhibited some axial variations in the lithium-ion mobility, these were not to the extent shown in Fig. 1. Consequently, we did in fact successfully fabricate from this crystal several 150 mm long detectors.

Detector Design

The detector structure used to fabricate the 300-element devices and the earlier prototype 30- and 60-element devices is shown schematically in Fig. 2. Here the pattern and guard-ring are located on the evaporated gold "blocking" contact, rather than on the lithium contact as is usually done. Selection of the gold contact rather than the lithium contact for the pattern was preferred because we wanted to achieve a high spatial resolution (i.e. 0.5 mm center-to-center spacing between elements). While this resolution could have been achieved employing the earlier reported etching techniques[8], we decided that this etching process could present yield problems for us. Consequently, the more conservative approach of evaporating the pattern through a mask was employed. However, this results in a lower interelement resistance than would occur if the pattern were on the lithium contact side.

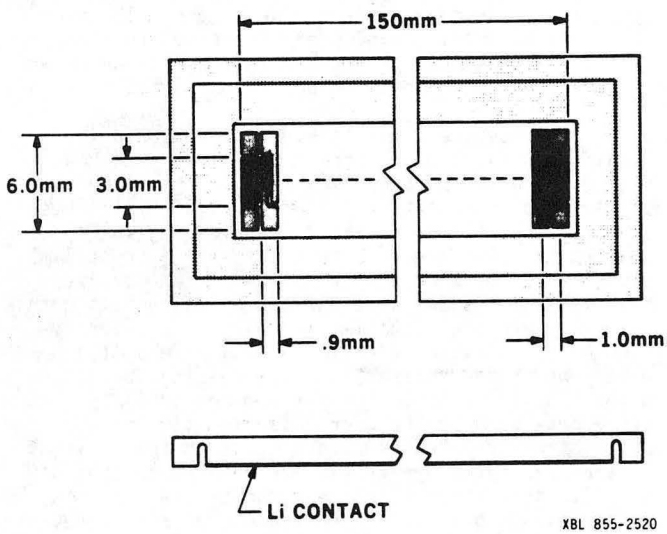

Fig. 2. Schematic representation of the geometry employed with the angiography detector. The 300-element device has an interdigitated structure with a 0.5 mm center-to-center strip spacing.

Interelement Resistance

Surface Resistance Measurements

To measure the interelement resistance on Si(Li) detectors, we employ the circuit shown schematically in Fig. 3. For the guard-ring device shown, the surface resistance between the central region and the guard-ring is determined by measuring the decrease in the current, I, with increasing series resistance R. The surface resistance, R_s, can then be estimated from:

$$R_s = \frac{R_A}{\frac{I_o}{I_A} - 1} \qquad (1)$$

where $I = I_o$ when $R = 0$ and $I = I_A < I$ when $R = R_A$. Figures 4a and b show the current, I, as a function of the resistance, R, measured on structures with similar dimensions on the lithium contact (N^+) and on the gold contact (P^+) sides of a Si(Li) detector. Also shown in these figures is the locus of the surface resistance, R_s, with the bias voltage, V_b, as a parameter.

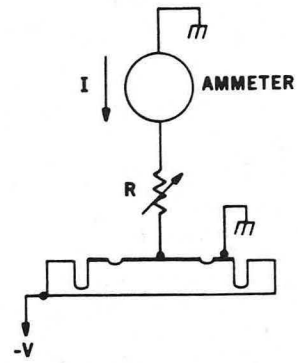

Fig. 3. Schematic drawing of the circuit used to measure the interelement resistance. In the actual circuit the current meter is a high gain feedback operational amplifier with low offset voltage and current.

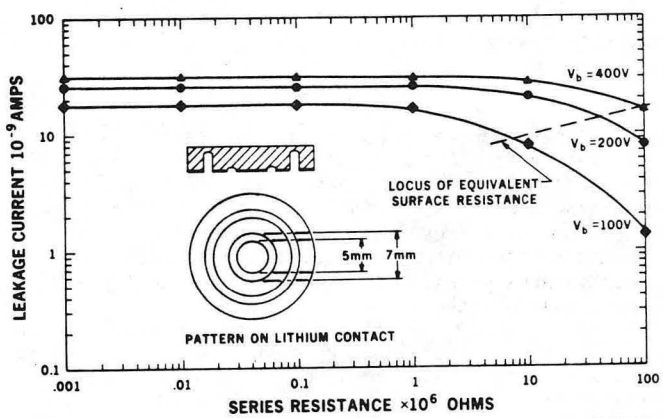

Fig. 4(a).

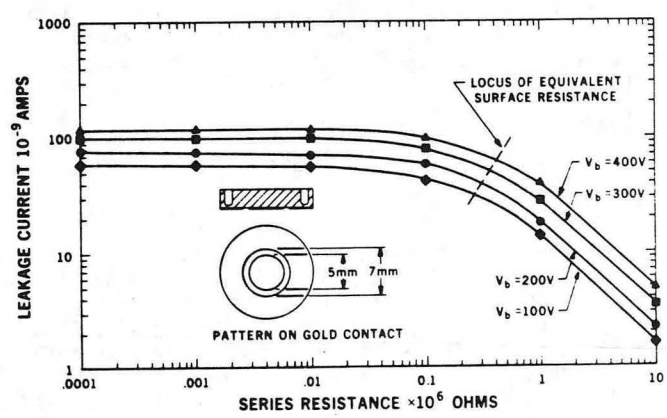

Fig. 4(b).

Fig. 4. Leakage current on the central region of the device shown in the insert as a function of the series resistance, R, of Fig. 3. Fig. 4(a) shows this current for a guard-ring structure on the lithium (N^+) side of a Si(Li) detector while 4(b) shows this current for the structure on the gold contact side (P^+). The calculated surface resistance between the center and guard is also shown.

Detector Surface Resistance

From the above figures it is evident that both the magnitude of the surface resistance and its sensitivity to the applied bias are different for these two structures. Earlier work by W.L. Brown[9] on germanium surfaces showed that the conduction along the surface is due to electrons attracted to the surface region by the fixed positive charge on the nascent semiconductor surface. Employing this model, the essential features of Figs. 4(a) and (b) can be explained.

With the N^+ structure of Fig. 4(a), increasing bias extends the depletion region deeper into the semiconductor allowing the electric field lines from the positive surface charge to terminate either on the acceptor centers present in the detector or on the negative charge centers present on the P^+ contact. Thus, increasing the bias leads to a decrease in the electron density near the surface. With sufficient bias, the electrons at the surface are totally depleted, the surface resistance becomes very high, and surface is said to be "pinched off"[10].

In contrast to the N^+ structure, increasing bias with the P^+ structure of Fig. 4(b) leads to a narrowing of the depletion region induced by the fixed positive surface charge. Further, there is no reduction in the electron density near the surface. Consequently, while the surface resistance does increase due to the narrowing of the depletion region, the surface never "pinches off" as it does with the N^+ structure.

The surface resistivity, ρ_s, can be estimated for the P^+ structure of Fig. 4(b) as:

$$\rho_s = 2\pi R_s / \ln(d_2/d_1) \text{ ohms}/\square \qquad (2)$$

where R_s is the surface resistance of Eq. 1 while d_2 and d_1 are the dimensions 7 mm and 5 mm of the pattern shown in the insert on the figure. From Eq. 2, $\rho_s = 7.5 \times 10^6$ ohms/□.

Using this resistivity value, we calculated an interelement resistance of about 65 K ohms for the 150 mm detector pattern of Fig. 2. Our measured values on the 150 mm device were about 70 - 80 K ohms, which are in good agreement with the calculated value. This low resistance in parallel with the signal source would present a serious limitation in the noise performance if these detectors were used with a charge-sensitive preamplifier[11]. However, here we are detecting the current produced by the incident radiation[12] and consequently, the 70 - 80 K ohm parallel resistance is large compared to the current-sensitive preamplifier input resistance. While use of the current mode accomodates the low parallel resistance, the leakage current from each element becomes of concern.

Detector Leakage Current

Room Temperature Leakage Current

The total detector leakage current measured on several of the 150 mm long detectors was of the order of 15 μA with 600 volt bias. However, the average leakage current on the individual elements was about 10 nA. Thus the majority of the leakage current was being carried by the guard ring on the device, as was expected. If we assume that the leakage current on the individual elements is due to bulk generation, then the effective lifetime in the depletion region, τ_0, can be estimated from[13]:

$$i = \frac{n_i W}{2\tau_0}$$

where n_i is the intrinsic carrier concentration and W is the depleted volume. From this we estimate $\tau_0 = 3$ ms which is a reasonable value for this parameter. Further we did not observe any variation in the element leakage current which we could ascribe to the presence of defects as discussed earlier. Consequently, it would appear that the defects which are reducing the lithium mobility have either been compensated by the lithium ions or are just not electrically active in the leakage current generation process.

Cooled Operation

For use at the Stanford Synchrotron Radiation Laboratory (SSRL), the detector was packaged as shown in Fig. 5. The flexible printed circuit harness facilitated the installation of the detector into a vacuum chamber in which a single stage thermoelectric cooler was mounted. Using this cooler with a drive of 25 watts we obtained a detector operating temperature of -29°C. At this temprature, individual element leakage currents of about 100 pA are expected; the actual measurement of these currents is difficult due to the low interelement resistance. During x-ray imaging operations, the average signal current produced by the incident 33 keV x-rays is about 500 nA/element. Therefore since the leakage current is less than 1% of the signal current and is constant during the scan, its effect on the image quality is negligible.

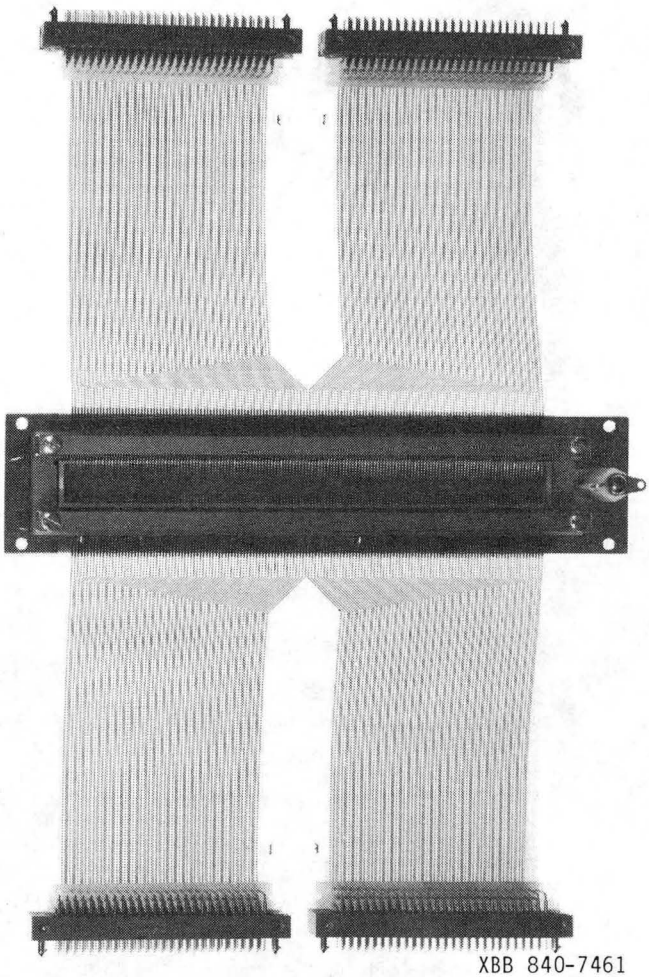

XBB 840-7461

Fig. 5. The 300-element detector with mounting hardware. Connection is made to the detector through spring wire contracts which in turn are connected to the flexible printed circuit harness.

Applications

The performance of the 300-element detector and associated electronics has by now been assessed in two

developmental tests at SSRL. The experimental arrangement used is similar to that of the earlier evaluations conducted with the 30- and 60-element designs. As before, two projection images are acquired, one image taken with the x-ray beam energy 72 eV below the iodine K absorption edge (at 33.16 keV) and the second 72 eV above the K edge[14]. By taking the logarithmic difference between these two images, a final image is obtained which has very high sensitivity to iodine but little sensitivity to soft tissue or bone if present.

In Fig. 6, a subtracted image obtained with the 300-element detector of the arterial tree in an excised pig's heart is shown. The arteries in this heart were filled with an ethiodol-vasaline mixture having an iodine concentration of 20 mg/cm^3. This concentration is similar to that expected in clinical use with peripheral venous iodine injection. The arteries in this figure are imaged with good resolution and very low background. Experiments are currently underway to image living canine hearts with the goal of obtaining human subject images in 1986.

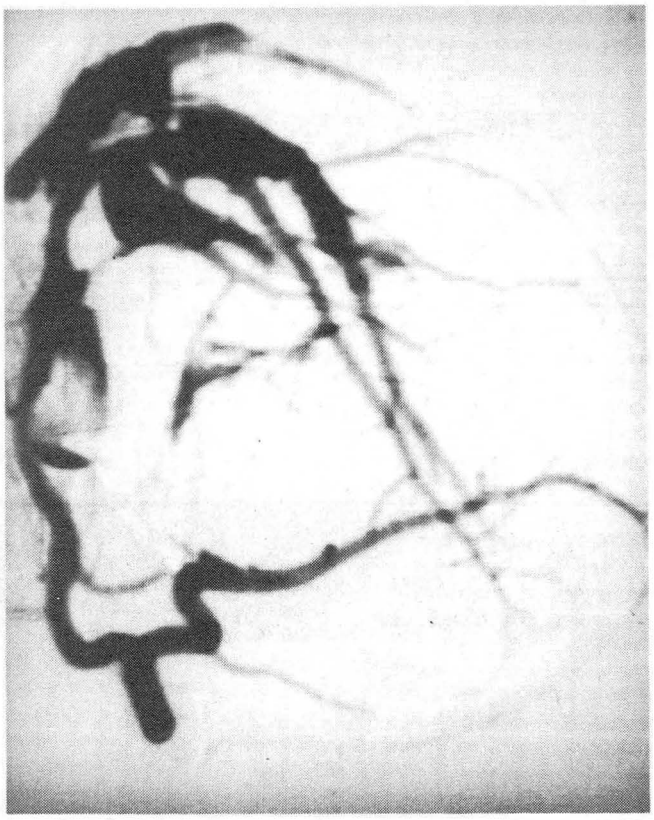

XBB 859-7210

Fig. 6. An angiograph of the arterial tree of an excised pig's heart obtained using the 300-element detector. The arteries in the heart were filled with iodine at 20 mg/cm^3 which is the anticipated clinical concentration. Some extravastion of the iodine occurred during the filling of the arteries of this heart. The damaged arteries appear in the upper left hand corner of the figure.

Conclusions

The observed variations in the lithium-ion mobility in the silicon crystal employed in the fabrication of these 300-element detectors point out one of the hazards of attempting to make large-area detectors. While we believe that the reduced mobility is due to mechanically induced B-swirl defects rather than to the presence of impurities, we have at the present time no convenient way of detecting these defects prior to detector fabrication. Consequently, without knowing the defect density, fabrication of large detectors as reported here will continue to be problematic.

Our results on the surface resistance on Si(Li) detectors clearly show a substantial difference in the resistance between the surfaces which can be "pinched off" and those that cannot. For applications where spectral resolution is of prime importance, the relatively low resistance associated with the Si(Li) P^+ contact would present a serious noise limitation.

Since the angiographs are produced by measuring the current change due to the incident x-rays in each detector element, the images are relatively insensitive to the presence of crystal defects which can cause charge trapping. The effects of trapping are more readily apparent in x-ray spectroscopy where the energy of each incident photon is measured. We have not, at this time, evaluated the effects of the crystal defects described in a spectrographic application.

Acknowledgments

We would like to thank F.S. Goulding for his ongoing interest in Si(Li) detector fabrication, D.A. Landis and N. Madden for their assistance with the electronics associated with this project, and W. Searles for his design and assembly of the cryostat.

This work was supported in part by the Director's Office of Energy Research, Office of Health and Environmental Research, U.S. Dept. of Energy under Contract DE-AC03-76SF00098, the William Randolph Hearst Foundation, the National Science Foundation under Contract DMR 77-27489 (for the operation of SSRL), and U.S. Dept. of Energy Contract DE-AC03-84ER-60200.

References

1. A.C. Thompson, F.S. Goulding, H.A. Sommer, J.T. Walton, E.B. Hughes, J. Rolfe and H.D. Zeman, IEEE Trans. Nucl. Sci. NS-29, 793 (1982).

2. A.C. Thompson, J. Llacer, L.C. Finman, E.B. Hughes, J.N. Otis, S. Wilson and H.D. Zeman, Nucl. Instr. and Meth. 222, 319 (1984).

3. W.L. Hansen and F.S. Goulding, Nucl. Instr. and Meth. 29, 345 (1964).

4. J.T. Walton and E.E. Haller, in: Nuclear Radiation Detector Materials, E.E. Haller, H.W. Kraner and W.A. Higinbotham, eds., North Holland, 1983, p. 141.

5. P.A. Iles and P.J. Coppen, J. Appl. Phys. 29, 1514 (1958).

6. A. Fong, J.T. Walton, E.E. Haller, H.A. Sommer and J. Guldberg, Nucl. Instr. and Meth. 199, 623 (1982).

7. H.J. Guislain, W.K. Schoenmaekers and L.H. Delaet, Nucl. Instr. and Meth. 101, 1 (1972).

8. P.N. Luke, IEEE Trans. Nucl. Sci. NS-31, No. 1, 312 (1984).

9. W.L. Brown, Phys. Rev. 91, No. 3, 518 (1953).

10. J. Llacer, IEEE Trans. Nucl. Sci. NS-11, No. 3, 345 (1964).

11. A.B. Gillespie, in: Electronics for Nuclear Particle Analysis, L.J. Herbst, ed., Oxford University Press, 1970.

12. H.D. Zeman, E.B. Hughes, L.E. Campbell, R. Hofstadter, R.L. Kirk, T.J. Krolicki, J. Rolfe, J.P. Stone, S. Wilson, E. Rubenstein, A.C. Thompson and J.T. Walton, IEEE Trans. Nucl. Sci. NS-29, 442 (1982).

13. A.S. Grove, Physics and Technology of Semiconductor Devices, John Wiley and Sons, 1967.

14. E.B. Hughes, E. Rubenstein, H. D. Zeman, G.S. Brown, M. Buchbinder, D.C. Harrison, R. Hofstadter, R.S. Kernoff, J.N. Otis and A.C. Thompson, Proc. of Synchrotron Radiation Instrumentation Conf. at Stanford University, July 1985, to be published in Nucl. Instr. and Methods.

This report was done with support from the Department of Energy. Any conclusions or opinions expressed in this report represent solely those of the author(s) and not necessarily those of The Regents of the University of California, the Lawrence Berkeley Laboratory or the Department of Energy.

Reference to a company or product name does not imply approval or recommendation of the product by the University of California or the U.S. Department of Energy to the exclusion of others that may be suitable.

TECHNICAL INFORMATION DEPARTMENT
LAWRENCE BERKELEY LABORATORY
UNIVERSITY OF CALIFORNIA
BERKELEY, CALIFORNIA 94720